Results from the NuMoon project: Tighter constraints on cosmic neutrinos above 10^22 eV from radio observations of the Moon

S. Buitink[*,††], J. Bacelar[†,‡‡], R. Braun[‡], G. de Bruyn[§,¶], H. Falcke[*], O. Scholten[†], K. Singh[†], B. Stappers[‖], R.Strom[§,] and R. al Yahyaoui[†]**

[*]*Radboud Univ. Nijmegen, Dept. of Astrophysics, IMAPP, P.O.Box 9010, 6500 GL Nijmegen*
[†]*Kernfysisch Versneller Instituut, University of Groningen, 9747 AA, Groningen, The Netherlands*
[‡]*CSIRO-ATNF, P.O.Box 76, Epping NSW 1710, Australia*
[§]*ASTRON, 7990 AA Dwingeloo, The Netherlands*
[¶]*Kapteyn Institute, University of Groningen, 9747 AA Groningen, The Netherlands*
[‖]*School of Physics & Astronomy, Alan Turing Building, Univ. of Manchester, Manchester, M13 9PL*
[**] *Astronomical Institute 'A. Pannekoek', University of Amsterdam, 1098 SJ, The Netherlands*
[††] *now at: Lawrence Berkeley National Laboratory, Berkeley, California 94720*
[‡‡]*now at: ASML Netherlands BV, P.O.Box 324, 5500 AH Veldhoven, The Netherlands*

Abstract. **UHE neutrinos and CRs initiate particle cascades underneath the lunar surface. These cascades have a negative charge excess and radiate Cherenkov radio emission in a process known as the Askaryan effect. The optimal frequency window for observation of these pulses with radio telescopes on the Earth is around 150 MHz. By observing the Moon with the Westerbork Synthesis Radio Telescope array we are able to set a new limit on the UHE neutrino flux. The PuMa II backend is used to monitor the Moon in 4 frequency bands between 113 and 175 MHz with a sampling frequency of 40 MHz. The narrowband radio interference is digitally filtered out and the dispersive effect of the Earth's ionosphere is compensated for. A trigger system is implemented to search for short pulses. By inserting simulated pulses in the raw data, the detection efficiency for pulses of various strengths is calculated.**

With over fourty hours of observation time, we are able to set a limit on the UHE neutrino flux. This new limit is an order of magnitude lower than existing limits. In the near future, the digital radio array LOFAR will be used to achieve an even lower limit.

Keywords**: UHE neutrino flux limits - radio detection - lunar cherenkov**

I. Introduction

When cosmic rays (CRs) or neutrinos hit the Moon they will interact with the medium. CRs will start a particle cascade just below the lunar surface, while neutrinos will interact deeper inside the Moon, also creating a hadronic shower. The negative charge excess of a particle cascade inside a dense medium will cause the emission of coherent Cherenkov radiation in a process known as the Askaryan effect [1]. This emission mechanism has been experimentally verified at accelerators [2][3] and extensive calculations have been performed to quantify the effect [4][5].

Radio telescopes on Earth can be used to search for lunar Cherenkov pulses of ultra-high energy (UHE) neutrinos and CRs. The idea was proposed by Dagkesamanskii and Zheleznyk [6] and the first experimental endeavors in this direction were carried out with the Parkes telescope [7], at Goldstone (GLUE) [8], and with the Kalyazin Radio Telescope [9].

Falcke and Gorham [10] suggested to use low-frequency telescopes (like LOFAR) for such an experiment. It was shown by Scholten et al. [11] that observing at lower frequencies has the distinct advantage that radio pulses have a much higher chance of reaching the observer, as will be explained in the next section. In this work we use data recorded with the Westerbork Synthesis Radio Telescope (WSRT) in the frequency range of 113-168 MHz to set limits on the neutrino flux.

II. Detection principle

UHE neutrinos or CRs interact below the lunar surface. In the case of a CR, all energy is converted into a hadronic shower. In a neutrino interaction, only about 20% of the energy is converted into a hadronic shower, while the other 80% is carried off by a lepton (corresponding to the neutrino flavor), which will not produce any observable radio emission. Muons will not produce enough charge density, while electromagnetic showers become elongated at energies above $E_{LPM} = 10^{18}$ eV due to the Landau-Pomeranchuk-Migdal (LPM) effect [12]. For these showers the angular spread of the radio emission around the Cherenkov angle becomes very small, severely lowering the chance of detection.

The lateral size of the cascade is of the order of 10 cm so the radio emission is coherent up to ~ 3 GHz. Former experiments, like GLUE, have observed at high frequencies (2.2 GHz) where the emission is strongest. For lower frequencies, however, the angular spread of

the emission around the Cherenkov angle increases due to diffraction. For emission at the Cherenkov angle, only those showers can be observed that hit the rim of the Moon, under such an angle that the emission will not be internally reflected at the lunar surface. With a larger angular spread in the emission, a wider range of geometries is allowed and a larger part of the lunar surface acts as a radiation source. When the wavelength is of the order of the shower length, several meters, the emission becomes nearly isotropic and pulses can be expected to come from the whole Moon [11]. In our experiment we exploit the range around 150 MHz, which is optimal for the highest energy events.

The regolith is the top layer of the Moon and consists of dust and small rocks. The properties of this layer are known from samples brought from the Moon by the Apollo missions [13]. The average index of refraction is $n = 1.8$ and the attenuation length is found to be $\lambda_r = (9/\nu[\mathrm{GHz}])$ m for radio waves [13][14]. The thickness of the regolith is known to vary over the lunar surface. At some depth there is a (probably smooth) transition to solid rock, for which the density is about twice that of the regolith. Wieczorek and Zuber [15] report that the density is almost homogeneous down to a depth of 20 km. In Scholten et al. [11] the effects of pure rock and regolith are simulated and found to give very similar detection limits for low frequencies.

III. Detection with WSRT

The Westerbork Radio Synthesis Telecope (WSRT) is an array telescope consisting of 14 parabolic telescopes of 25 m on a 2.7 km east-west line. The NuMoon experiment uses the Low Frequency Front Ends (LFFEs) which cover the frequency range 115–180 MHz. Each LFFE records full polarization data. For our observations we use the Pulsar Machine II (PuMa II) backend [16], which can record a maximum bandwidth of 160 MHz, sampled as 8 subbands of 20 MHz each. We use two beams of 4 bands each, centered around 123, 137, 151, and 165 MHz. The two beams are aimed at different sides of the Moon, each covering about one third of the lunar surface, in order to enlarge the effective aperture and create the possibility of an anti-coincidence trigger. A lunar Cherenkov pulse should only be visible in one of the two beams. Because of overlap in the subbands the total bandwidth per beam is 65 MHz. The system has a real time automatic gain control (AGC) system, that stabilizes the average gain of the output signal. For each subband, the time series data is recorded at several storage nodes with a sampling frequency of 40 MHz.

The data is processed in blocks of 0.1 s, each block being divided in 200 traces of 20 000 time samples. The signal of individual WSRT dishes is 2 bit, limiting the dynamic range of an 11-dish observation to 34. There is data for two beams, each containing 4 frequency bands and 2 polarization directions. The data analysis is performed in the following steps.

RFI background reduction: Radio Frequency Interference (RFI) is narrow band anthropogenic emission, which can be responsible for a large part of the received power and has to be filtered out of the data. For all time traces an FFT is produced and for each data block the 200 frequency spectra are added to obtain an integrated frequency spectrum. A 9th order polynomial function is fitted to this spectrum to fit the baseline and bins containing a value exceeding the fit by 50% are marked as RFI lines. In each individual frequency spectrum all bins that are marked as RFI lines are set to zero. This procedure is carried out separately for the 4 frequency bands and the 2 polarizations. The number of RFI lines per spectrum varies with time and is different for all frequency bands and polarizations, but does seldom exceed 200. The corresponding loss in bandwidth is approximately 2% at maximum.

Ionospheric de-dispersion: As the radio signal propagates through the Earth's ionosphere it is dispersed. A de-disperion is performed by applying a frequency dependent phase shift to the data before transforming back to the time domain. The vertical Total Electron Content (TEC) values, that are needed for the de-dispersion, are provided by the DLR Institut für Kommunikation und Navigation[1] and the slanted TEC (STEC) values are calculated by compensating for the elevation of the Moon. Because of variations in the thickness of the ionosphere on short timescales and over distance, we assume the presence of an error in the de-dispersion, resulting in an increased time width of the pulses and an offset between the arrival times of pulses in different frequency bands.

Evaluation of P_5: After de-dispersion, the data is transformed back into the time domain. Next, we calculate P_5, the power integrated over 5 consecutive samples normalized over one trace:

$$P_5 = \frac{\sum_{5 \text{ samples}} P_x}{\left\langle \sum_{5 \text{ samples}} P_x \right\rangle} + \frac{\sum_{5 \text{ samples}} P_y}{\left\langle \sum_{5 \text{ samples}} P_y \right\rangle}, \quad (1)$$

where the averaging is done over one time trace (20 000 time samples), and x and y denote the two polarizations. The integration has been chosen to be over 5 samples, because this is the typical number of samples over which the power is spread for a bandwidth limited and Nyquist sampled pulse with a small dispersion.

Pulse search: The data is scanned for values of P_5 exceeding 5. The band with the highest frequency is first scanned for P_5 values exceeding 5. When such a value is found the P_5 values of the other 3 frequency bands are evaluated near this position. Between pulses in the different bands, a time shift is allowed based on an error of 30% on the STEC value. When a P_5 value exceeding 5 is found in all bands the time trace is permanently stored, together with information on the RFI lines and

[1] http://www.dlr.de/kn

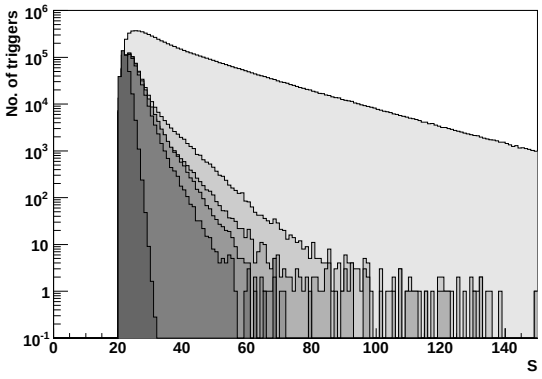

Fig. 1: Distribution of S for several cuts. The lines enclosing different shades of grey represent different cuts. From light to dark they represent the distribution of raw triggers, T cut, TW cut, TA cut, TWA cut, and pure Gaussian noise.

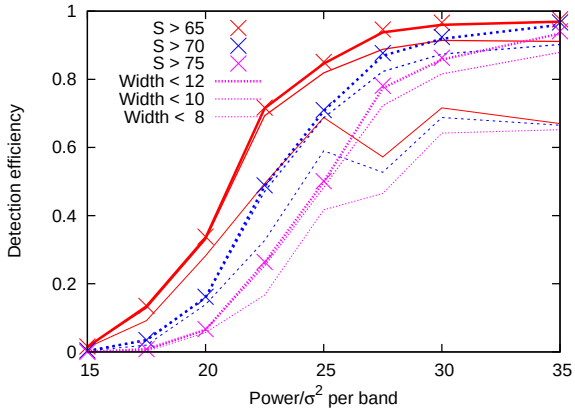

Fig. 2: Detection efficiency against pulse strength. The color correspond to different thresholds and the thickness correspond to different maximum widths.

the data of the corresponding time trace in the other beam. For each trigger the location, maximum value, width and offsets between locations in the different bands are stored. The width is defined as the number of consecutive P_5 values that exceed 5. The value S is defined as the sum over the maximum P_5 values in the 4 frequency bands:

$$S = \sum_{4 \text{ bands}} P_5. \quad (2)$$

IV. Observations

In the period between June 9, 2007 and November 11, 2008, 22 successful observation runs have been performed, corresponding to an effective observation time of 46.7 hours.

Fig. 1 shows the distribution of S. The line enclosing the area of the lightest shade of grey corresponds to the raw triggers. Several additional cuts can be applied:

Timer signal (T): The data contains short strong pulses that repeat at a regular interval of 102.4 s, suggesting a technical origin. Cutting out the time intervals in which these pulses occur corresponds to a loss of $\sim$10% of observation time.

P_5 width (W): The number of consecutive P_5 values exceeding the threshold should be limited for a real lunar pulse. Fig. 1 shows the distribution corresponding to triggers for which the width is smaller than 10 in all four frequency bands (including a cut on the timer signal).

Anti-coincidence (A): A lunar pulse should be visible in only one of the two beams. An anti-coincidence trigger is set up by excluding events in which a pulse was found in both beams in the same time trace. Fig. 1 includes distributions of S after application of only the timer and width cut (TW), only the timer and anti-coincidence cut (TA), and a combination of all cuts (TWA).

The line enclosing the darkest area in Fig. 1 corresponds to the distribution of triggers that are expected if the background is pure Gaussian noise. After all cuts have been applied the number of triggers for which $S > 23$ is a factor of 3-4 higher than the amount of triggers expected for Gaussian noise, while the largest S value in the distribution is about twice as large as the largest S value for Gaussian noise.

V. Simulations

The efficiency with which pulses are found by the analysis procedure and the effects of data cuts and ionospheric dispersion are simulated by adding pulses to raw data. These pulses are delta peaks inserted at random time with a random phase. Because of the sampling, the bulk of the power in such a pulse typically spreads out over a few time samples. For the simulations we have inserted 1000 pulses in a 10 seconds segment of raw WSRT data.

We define the detection efficiency (DE) as the fraction of inserted pulses that is retrieved after applying the trigger conditions and the cuts that are used in the analysis. Fig. 2 shows the DE for inserted pulses of varying strength. The power is expressed in σ^2, which is defined as the mean value of P_5. The pulses are dispersed with STEC=10 and reconstructed with STEC=12 to include a practically unavoidable error. Due to interference with the background the recovered pulse strength differs from the input value. The data point (crosses) show the DE without any width cut applied. Different colors (linestyles) correspond to different detection thresholds, while the thickness of the line indicates the cut on width (thickest line for $W < 12$, medium thickness $W < 10$ and thinnest line $W < 8$).

From Fig. 2 it can be seen that the DE tends to saturate to unity for large pulses. However one also sees that the width cut may severely limit the DE which even worsens with increasing input pulse strength. The reason for this is that with increasing pulse strength the width (as defined in this work) increases. For really large pulses the signal may saturate causing an additional broadening of the recovered pulse.

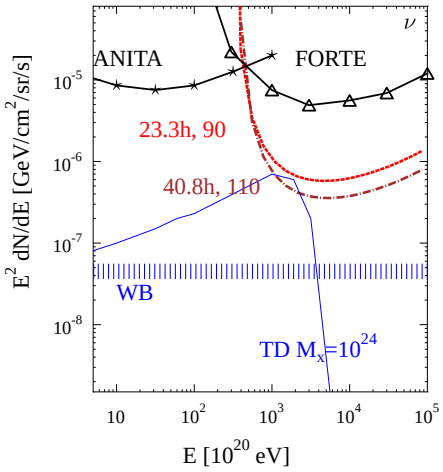

Fig. 3: Preliminary neutrino flux limit currently established with 46.7 hours of data. The red line is calculated for a minimum pulse strength of $4 \times 22.5 = 90\sigma^2$ ($t_{\rm eff}$ =23.3 hours), and the brown line for a minimum pulse strength of $4 \times 27.5 = 110\sigma^2$ ($t_{\rm eff}$ = is 40.8 hours).

VI. Background

For a radio antenna, the 1 σ noise power density is given by:

$$F_n = \frac{2kT_{\rm sys}}{\sqrt{\Delta t \Delta \nu} A_{\rm eff}} 10^{26} \text{Jy}, \qquad (3)$$

where k is the Boltzman constant (1.38×10^{-23} Joules), $T_{\rm sys}$ is the antenna effective temperature in Kelvin, Δt and $\Delta \nu$ are the time and frequency bins of the measurement, and $A_{\rm eff}$ is the effective area of the telescope in m^2. For the Westerbork antennas we used, $A_{\rm eff} = 491$ m^2. For the measuring band which we need, the LFFE measuring between 113 and 170 MHz, one has $T_{\rm sys}$ of 400 - 700 K. We use 11 antennas, yielding for the noise power per Nyquist time sample ($\Delta t \Delta \nu = 0.5$), $F_n = 349(T_{\rm sys}/491)$ Jy.

VII. Results

We present preliminary results of 46.7 hours of data in which no triggers were found with $S > 70$. The fraction of pulses of a certain power that is retreived after applying the trigger conditions and various cuts is given by the simulated DE (see Fig. 2). The effective observation time $t_{\rm eff}$ is defined as the DE times the total amount of observation time (corrected for time loss due to cuts). Different points on the line corresponding to $S > 70$ and width< 10 in Fig. 2 give different flux limits. For example, pulses of a power of $27.5\sigma^2$ per frequency band have a detection efficieny of 87.5%, meaning no pulses above this power have been found in $t_{\rm eff}$ =40.8 hours. Alternatively, a DE of 50% is reached for pulses of 22.5 σ^2 per frequency band. No pulses exceeding this power have been found in $t_{\rm eff}$ =23.3 hours.

Fig. 3 shows the limits for these two cases. For the pulses of 27.5 σ^2 per frequency band, the limit is 220 kJy. For pulses of 22.5 σ^2 per frequency band, the limit is 180 kJy. In both cases a bandwidth of 55 MHz is used. The first choice gives the more constraining limit. At the energy of $5 \cdot 10^{23}$ eV the neutrino flux is less than $8 \cdot 10^{-22}$ cm^{-2}sr^{-1}s^{-1}.

The current limits in the UHE region are established by ANITA [17] and FORTE [18]. The Waxman-Bahcall limit [19] and a top-down (TD) model [20] for exotic particles of mass $M_X = 10^{24}$ eV, are also included

The next phase in the NuMoon experiment will be to use LOFAR, the Low Frequency Array [21], that is under construction in the Netherlands. LOFAR is a network of low frequency omni-directional radio antennas communicating over a fiber optics network. It will feature two types of antennas operating at different frequencies: the Low Band (LB) antennas cover a band of 30–80 MHz while the High Band (HB) antennas cover the regime 110–240 MHz. The latter will be used for the NuMoon observations. LOFAR is organized in 35 stations each containing 48 LB and 96 HB antennas. Half of the stations are located inside the 2 km$\times$3 km core with a total collecting area of $\sim$0.05 km^2. Multiple beams can be formed to cover the surface of the Moon, resulting in a sensitivity that is about 25 times better than the WSRT [22].

Eventually, the best sensitivity will be achieved with the Square Kilometer Array [23] (SKA), planned to be completed in 2020. The Australian SKA Pathfinder (ASKAP) is expected to be operational around 2011. A study of the sensitivity of ASKAP, SKA and the Australia Telescope compact Array (ATCA) can be found in James et al. [24]

References

[1] G.A. Askaryan, Sov. Phys. JETP, 14, 441, 1962
[2] D. Saltzberg et al., Phys. Rev. Lett., 86, 2802, 2001
[3] P.W. Gorham et al., Phys. Rev. E, 62, 8590, 2000
[4] E. Zas, F. Halzen and T. Stanev, Phys. Rev. D, 45, 362, 1992
[5] J. Alvarez-Muñiz and E. Zas, Phys. Lett. B, 411, 218, 1997
[6] R.D. Dagkesamanskii and I.M. Zheleznyk, Sov. Phys. J.E.T.P., 50, 233, 1989
[7] T.H. Hankins, R.D. Ekers and J.D. O'Sullivan, MNRAS, 283, 1027, 1996
[8] P. Gorham et al., Phys. Rev. Lett., 93, 41101, 2004
[9] A. Beresnyak et al., Astronomy Reports, 49, 127, 2005
[10] H. Falcke and P. Gorham, Astropart. Phys., 19, 477, 2003
[11] O. Scholten et al.Astropart. Phys., 26, 219, 2006
[12] J. Alvarez-Muñiz and E. Zas, Phys. Lett. B, 434, 396, 1998
[13] G.R. Olhoeft and D.W. Strangway, Earth Plan. Sci. Lett., 24, 394, 1975
[14] G. Heiken, D. Vaniman and B.M. French, "Lunar Sourcebook, A users guide to the Moon", Cambridge Univ. Press, 1991
[15] M. Wieczorek and T. Zuber, Geophys. Res. Lett., 28, 4023, 2001
[16] R. Karuppusamy, B. Stappers, W. van Straten, astro-ph/0802.2245v1
[17] S.W. Barwick et al., Phys. Rev. Lett., 96, 171101, 2006
[18] N.G. Lethinen, P.W. Gorham, A.R. Jacobson, R.A. Roussel-Dupre, Phys. Rev. D, 69, 013008, 2004
[19] J. Bahcall and E. Waxman, Phys. Rev. D, 64, 64, 2001
[20] R.J. Protheroe, T. Stanev, Phys. Rev. Lett., 77, 3708, 1996
[21] H. Falcke et al., Long Wavelength Astrohysics, 26th meeting of the IAU, Prague, 2006
[22] K. Singh et al., Proc. of 21th ECRS, 2008
[23] http://www.skatelescope.org/ SKA website
[24] C. James and R. Protheroe, astro-ph/08023562v1